Scientia Iranica D (2021) 28(3), 1685–1697

Sharif University of Technology
Scientia Iranica
Transactions D: Computer Science & Engineering and Electrical Engineering
http://scientiairanica.sharif.edu

Complex dynamics of a Fitzhugh-Rinzel neuron model considering the effect of electromagnetic induction

Z. Wang[a], P. Zhang[a], I. Moroz[b], and A. Karthikeyan[c,1,*]

a. *Shaanxi Engineering Research Center of Controllable Neutron Source, School of Science, Xijing University, Xi'an 710123, China.*
b. *Mathematical Institute, University of Oxford, Andrew Wiles Building, Oxford, UK.*
c. *Nonlinear Systems and Applications, Faculty of Electrical and Electronics Engineering, Ton Duc Thang University, Ho Chi Minh City, Vietnam.*

Received 16 January 2021; received in revised form 31 March 2021; accepted 24 May 2021

KEYWORDS
FH-R neuron model;
Stability analysis;
Bifurcation diagram;
Dynamical network;
Wave propagation.

Abstract. Different single-neuron computational models have been proposed in different pieces of the literature. Most of these models belong to the Hodgkin-Huxley (H-H) type, which facilitates producing complex neuron behavior and ensures efficient computational cost. In this paper, a modified FitzHugh-Rinzel (FH-R) model considering the effect of magnetic induction was proposed. Different features of the model were explored from a complex and nonlinear perspective. For instance, the impact of magnetic field on the stability of equilibrium points was studied using stability analysis. Bifurcation analysis indicated that the proposed neuron model enjoyed multistability. Furthermore, the spatiotemporal behavior of the proposed model was investigated in a complex network consisting of FH-R oscillators. The effect of external stimuli on wave propagation in the network was explored.

1. Introduction

Chaos and fractal geometry are known as key factors in modeling the alpha rhythm of the brain and nervous system. Considering these factors helps design a more accurate model of neurological disease [1]. It is claimed that the brain's electrical activities are chaotic. Moreover, fractal geometry can be utilized to model a large population of interactive neurons crowded in the brain [1–3]. A horde of models was developed to understand and grasp the perplexing design of the brain. One of the fundamental and well-known neuron oscillators is the Hodgkin-Huxley (H-H) model [3], in which the axon electrical activities of a squid's nerve cell were studied. This model is composed of four differential equations with eight auxiliary algebraic functions. The variables of the H-H model include membrane potential, ionic currents, and inactivation of Na channel. The H-H model parameters are biologically significant and measurable. There are many H-H type models in the literature known as the conductance-based neuronal models [3–5]. The complexity of these models is lower than the H-H model which allows scientists to explore the synaptic and dendritic effects [6], the interplay between ionic currents [7], thermal [8] and photosensitive effects on excitability of the neuron [9,10], and other topics related to the dynamics of a single cell [11]. These models can reasonably predict the response of

1. *Present address: Electronics and Communication Engineering, Prathyusha Engineering College, Thiruvallur, Tamil Nadu 602025, India.*
*. *Corresponding author.*
E-mail address: mrs.anithakarthikeyan@gmail.com (A. Karthikeyan)

doi: 10.24200/sci.2021.57547.5295

an individual neuron to external stimulation; however, this prediction turned out to be too complicated for modeling two- and three-dimensional arrays of connected neurons [12].

In H-H equations, membrane potential (V) and sodium current (m) variables undergo rapid changes compared with potassium (n) and inactivation of Na current (h). Upon setting slowly changing variables constant arbitrarily, Fitzhugh proposed a two-dimensional neuron model in 1961 [13]. Alongside these reductions, using phase space analysis changes the above model into a practical, intricate neuron model. A year later, in 1962, in line with Fitzhugh, Nagumo's investigation reached the same results [14]. By including an externally supplied current (I), the Fitzhugh-Nagumo (FHN) model is presented. FHN model can potentially describe the qualitative nature of the neural activity and impulse propagation similar to the H-H model [15]. The homoclinic orbits of the FHN model from the fast-slow perspective were studied in [16]. Synchronization of both directed and undirected electrical couplings of neurons was discussed with the FHN model in [17]. Alongside the FHN neuron model, the synchronization of the network consisting of the H-H neuron model was presented in [18]. The bursting phenomenon in a coupled identical neuron was analyzed using the FHN model in [19]. Emergence of alternative chimeras in the coupled bursting neurons was explored in [20]. The collective behavior of hyper neural networks [21] and complex neural networks consisting of the number of sub-networks non-locally coupled with each other [22] was investigated. Oscillatory chaotic nature, especially chaotic spiking, referred to as firing death, was identified and studied in FHN oscillators in a network [23]. Most of the studies in the literature have investigated the various behaviors of FHN except the bursting nature of neurons. Chattering neurons in a cat neocortex [24] revealed fire periodic bursts of spikes when stimulated, which led to the brain oscillations in the gamma frequency [25,26].

To overcome the drawback of the FHN model, the FitzHugh-Rinzel (FH-R) model was proposed by adding a super slow variable. In [27,28], the spiking, bursting, and quiescent behavior of the FH-R model were studied. Networks of diffusively coupled neurons consist of FH-R oscillators exploring various complex dynamical behaviors and synchronization effects [29], especially the spatiotemporal pattern identified in coupled systems. A complex pattern with both subgroups of coherent and incoherent oscillators can emerge in networks known as chimeras. In [30–32], spiral waves in a network of phase-locked oscillators were reported as two-dimensional chimeras. Wave propagation in a network of dynamical oscillators was reported in both excitable [33] and noisy sub-excitable media [34].

2. Mathematical model

Fitzhugh and Rinzel introduced the FH-R model [35–37] by evolving the FHN neuron model. The traditional FHN model clearly explains the excitations and spike generations of a neuron but cannot replicate the firing patterns of cortical neurons [38]. In the case of the FH-R model, an additional slow subsystem was introduced alongside the regular FHN model. This new model could produce various firing activities to properly determine the related parameters. Here, a modified FH-R neuron model that considered the impact of magnetic field was proposed with a fourth-order differential equation as follows:

$$\begin{aligned}
&\dot{v} = v - \frac{v^3}{3} - w + y + I_{ext} - k_0 v(\alpha + \beta\phi^2),\\
&\dot{w} = \delta(0.7 + v - 0.8w),\\
&\dot{y} = \mu(c - y - v),\\
&\dot{\phi} - k_1 v - k_2\phi,
\end{aligned} \tag{1}$$

where v denotes membrane potential, w fast variable, y slow current, and ϕ impact of magnetic field on the membrane. There are six parameters in Model (1): I_{ext} is the external excitation current, δ the parameter controlling the fast subsystem, μ the parameter controlling the slow subsystem, k_0 the electromagnetic induction current's gain, $k_1 = \frac{1}{L}$ with L representing the turn number of the cells or media as L turns into coil for estimating magnetic field effect, and k_2 the cell leakage flux degree. The parameter c and the external current I_{ext} are taken as control variables in the entire discussion presented in the paper. The parameter values for System (1) include the following:

$$I_{ext} = 0.73, \quad \delta = 0.01, \quad \mu = 0.35, \quad c = -0.55,$$

$$\alpha = 0.1, \quad \beta = 0.03, \quad k_0 = 0.1,$$

$$k_1 = 0.01, \quad \text{and} \quad k_2 = 0.5.$$

In the paper, two cases are discussed: Case A for System (1) without electromagnetic induction and Case B for System (1) considering electromagnetic induction.

3. Stability analysis

3.1. Case A

First, the equilibrium states of Case A for the new FH-R model are determined. It is convenient to replace the numerical values of some of the parameters by arbitrary names:

$$\dot{v} = v - \frac{v^3}{3} - w + y + I_{ext} = F,$$

$$\dot{w} = P_4(P_1 + v + P_2 w) = G,$$

$$\dot{y} = P_5(c - y - v) = H, \tag{2}$$

where $P_1 = 0.7$, $P_2 = 0.8$, $c = -0.55$, $P_4 = \delta = 0.01$, $P_5 = \mu = 0.35$, and $I_{ext} = 0.73$.

In this study, I_{ext} and c are chosen as two bifurcation parameters by keeping other parameters fixed to their prescribed numerical values. The equilibrium points in Eq. (2) are calculated by setting the right-hand side of the equation to zero. Setting $H = 0$ gives $y = P_3 - v$, while setting $G = 0$ gives $w = \frac{v+P_1}{P_2}$. Substituting $F = 0$ yields a cubic equation for v as follows:

$$v^3 + \frac{3}{P_2}v + 3\left(\frac{P_1}{P_2} - c - I_{ext}\right) = 0. \tag{3}$$

Solving Eq. (3) leads to one real root for v when the external current ranges between $[-10, 10]$. For $-2.86552 \leq I_{ext} \leq 2.53188$, there is a pair of complex roots with nonzero imaginary parts. The equilibrium point in Eq. (2) for the chosen set of parameters is $(v^*, w^*, y^*) = (-0.51877, -0.22654, -0.3223E - 10)$. Figure 1 shows the absolute value of the equilibrium point for $0 \leq I_{ext} \leq 10$.

According to Figure 2, the parameter c varies in the range of $-1.5 \leq I_{ext} \leq 1.5$ and the remaining parameters are fixed to their prescribed values.

The third-order Jacobian matrix is utilized to analyze the local stability of the equilibrium point of the model as follows:

$$J = \begin{pmatrix} 1 - v^2 & -1 & 1 \\ P_4 & -P_2 P_4 & 0 \\ -P_5 & 0 & -P_5 \end{pmatrix}. \tag{4}$$

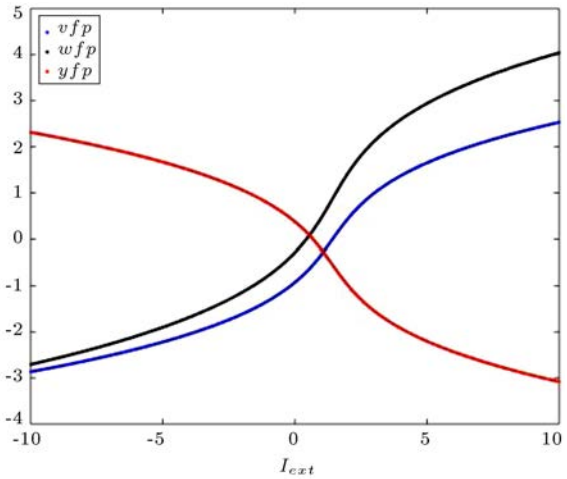

Figure 1. The different values of the fixed points of the neuron model in Case A (Eq. (2)) as I_{ext} varies. The blue, black, and red lines correspond to absolute fixed point values of v, w, and y. According to the results, increasing the value of I_{ext} leads to increasing both values of v, w but decreasing the value of y.

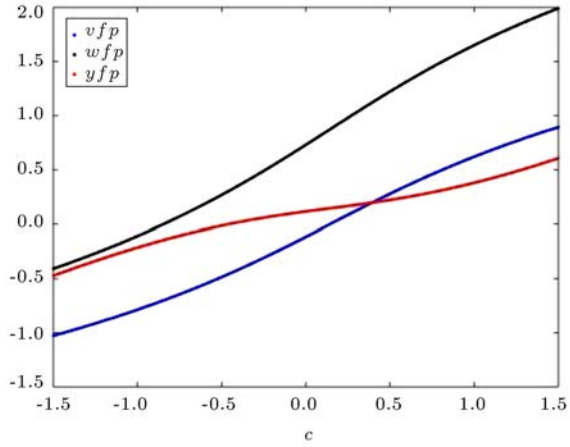

Figure 2. The different values of the fixed points of the neuron model (Eq. (2)) as c varies. The blue, black, and red lines correspond to absolute values of v, w, and y. Increasing the value of I_{ext} leads to increasing all values of v, w, and y.

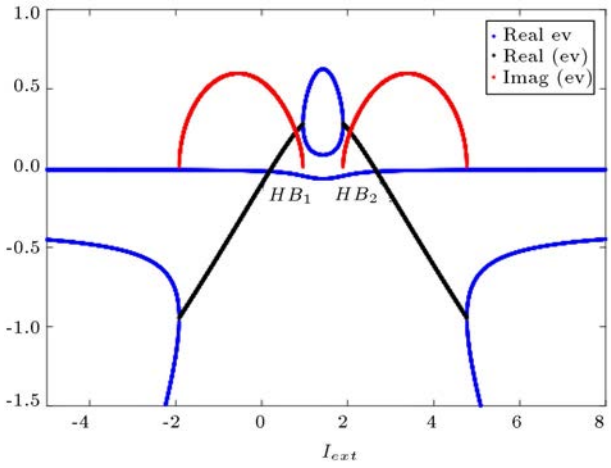

Figure 3. Eigenvalues of the equilibrium points of variable v by changing I_{ext}. The blue, black, and red curves correspond to the real and imaginary parts of the eigenvalues. The two Hopf bifurcation points, HB_1 at $I_{ext} = 0.226$ and HB_2 at $I_{ext} = 2.666$ are labeled where the black curve crosses the imaginary axis.

The cubic characteristic equation, the determinant of $J - \lambda I_3$, is:

$$\lambda^3 + A_2\lambda^2 + A_1\lambda + A_0 = 0, \tag{5}$$

where:

$$A_2 = P_2 P_4 + P_5 + v_e^2 - 1,$$

$$A_1 = P_4 + P_5 + P_2 P_4 P_5 + (1 - v_e^2)(P_5 + P_2 P_4),$$

$$A_0 = P_4 P_5(1 + P_2) + P_2 P_4 P_5(v_e^2 - 1). \tag{6}$$

Figure 3 shows a section of the plots of three eigenvalues for the characteristic equation (Eq. (5)) as I_{ext}

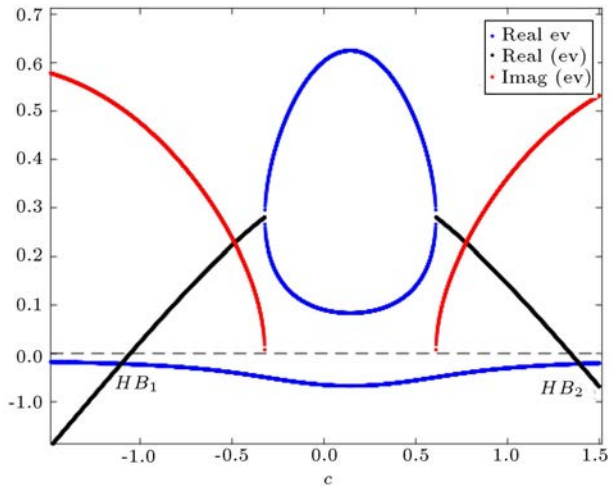

Figure 4. Eigenvalues of the equilibrium points of variable v by changing the c. The blue, black, and red curves correspond to the real and imaginary parts of the eigenvalues. The two Hopf bifurcation points, namely HB_1 at $c = -1.054$ and HB_2 at $c = 1.344$, are labeled where the black curve crosses the imaginary axis.

varies in the range of $[-10, 10]$, one of which is real and the others are complex.

There are two Hopf bifurcations in Figure 3, in which the real part of complex eigenvalues crosses the imaginary axis at $I_{ext} = 0.226$ and $I_{ext} = 2.666$. The frequencies at Hopf bifurcations are both equal to $\omega = 49247$. Figure 4 shows the corresponding plots when parameter c varies. Now, two Hopf bifurcations occur at $c = -1.054$ and $c = 1.344$, with frequencies again given by $\omega = 0.49247$.

Criteria for detecting the occurrence of Hopf bifurcation can be measured by substituting $\lambda = I\omega$ into Eq. (5). Assuming the same real and imaginary parts of the eigenvalues gives:

$$\omega^2 = \frac{A_0}{A_2} = A_1 > 0, \tag{7}$$

which meets the sufficient Hopf bifurcation criteria: $A_0 = A_1 A_2$. Since both c and I_{ext} appear in the expression for v_e, it is not easy to obtain the curve of Hopf bifurcations as a function of each of these two parameters analytically. However, the locations of the two Hopf bifurcations as well as their frequency values have an underlying symmetry.

Figure 5 shows the plots of $\omega_r^2 = \frac{A_0}{A_2}$ (blue points), $\omega_i^2 = A_1$ (red points), and the Hopf bifurcation condition $HB = A_1 A_2 - A_0$ when I_{ext} increases. Note that the symmetry of the Hopf Bifurcation points is about $I_{ext} = 1.199$, which is equal to the minimum value of $\omega_i^2 = 0.0048$. This symmetry explains why the frequencies at both Hopf bifurcation points are the same and equal to $\omega = 0.49248$. Moreover, the results of Figures 3 and 4 are verified by plotting bifurcation transition diagrams of the maxima of v in each cycle

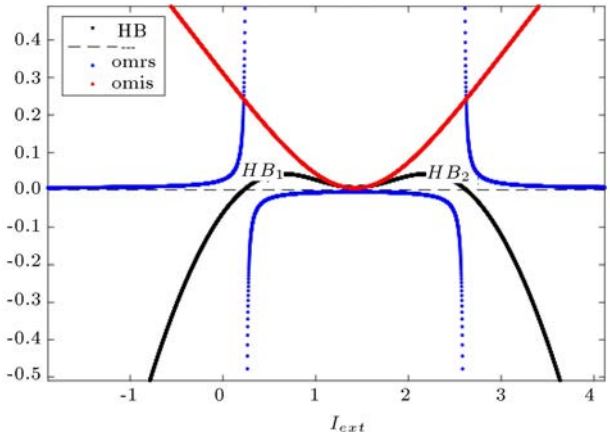

Figure 5. The behaviors of ω_r^2 (blue), ω_i^2 (red) and the Hopf bifurcation condition HB (black) as I_{ext} increases.

as I_{ext} (Figure 6(a)) and c increase (Figure 6(b)). In each plot, the two Hopf bifurcation points HB_1 and HB_2 are labeled. In each case, the values of these four points are consistent with those from the eigenvalue plots of Figures 3 and 4.

3.2. Case B

By including the effects of electromagnetic induction $\phi(t)$ into the FH-R system (Eq. (2)), four-dimensional nonlinear equations are obtained:

$$\begin{aligned}
&\dot{v} = v - \frac{v^3}{3} - w + y + I_{ext} - k_0 v(\alpha + \beta\phi^2) = F,\\
&\dot{w} = P_4(P_1 + v - P_2 w) = G,\\
&\dot{y} = P_5(c - y - v) = H,\\
&\dot{\phi} - k_1 v - k_2 \phi = K.
\end{aligned} \tag{8}$$

Additional parameters in Eq. (8) and their prescribed values are set to $\alpha = 0.1$, $\beta = 0.03$, $k_0 = 0.01$, $k_2 = 0.5$. The equilibrium state values are:

$$W_e = \frac{1}{P_2}(P_1 + V_e), \qquad Y_e = c - V_e, \qquad \phi_e = \frac{k_1}{k_2} V_e, \tag{9}$$

where V_e is the real solution to the modified cubic equation:

$$\left(1 + 3\frac{\beta k_0 k_1^2}{k_2^2}\right) V^3 + 3\left(\frac{1}{P_2} + k_0\alpha\right) V + 3\left(\frac{P_1}{P_2} - c - I_{ext}\right) = 0. \tag{10}$$

When $k_0 = k_1 = 0$, Eq. (2) of Case A can be recovered. The equilibrium points of Eq. (10) are shown in Figure 7(a) and (b) by varying the parameters I_{ext} and c in turn. In both cases, the variation of ϕ is too insignificant between $-0.572497242204E-10 < \phi_e < 0.505714997709E-01$ in Figure 7(a) and between

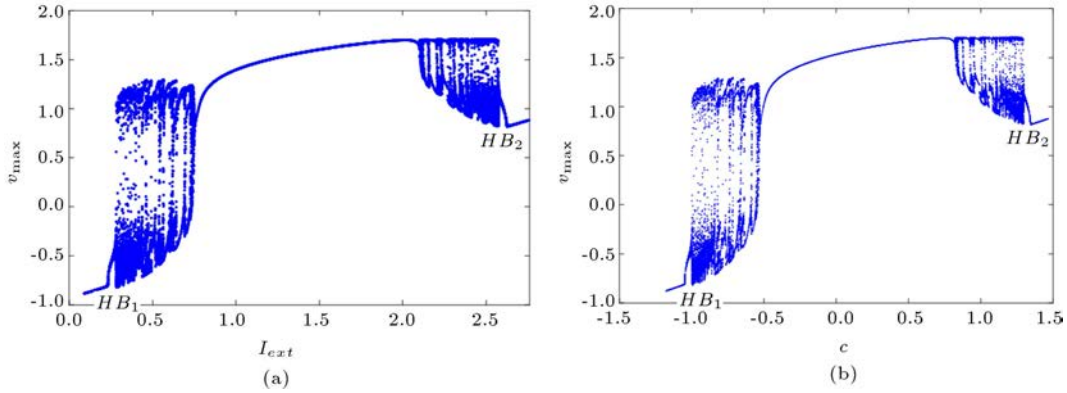

Figure 6. (a) The bifurcation transition plots according to the changing I_{ext} as a function of $v_{\max}$. (b) The bifurcation transition plots according to the changing c as a function of $v_{\max}$.

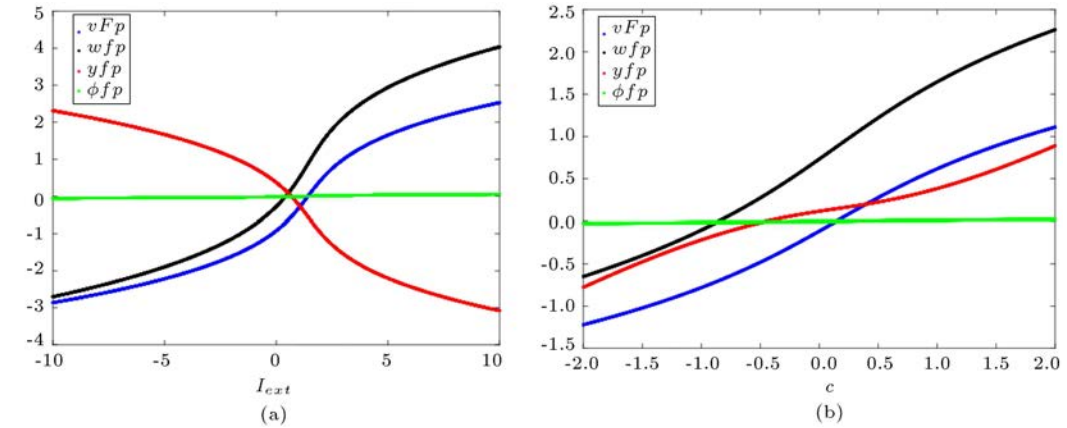

Figure 7. The different values of the fixed points of the neuron model (Eq. (10)) as: (a) I_{ext} and (b) c varies. The blue, black, red, and green lines correspond to absolute values of V_e, W_e, Y_e, and Φ_e.

$-0.244182952138E-01 < \phi_e < 0.222041836952E-01$ in Figure 7(b). The range is extended for c in order to capture the Hopf bifurcation values in Case B.

After performing the procedure for Case A, the linear stability of the real equilibrium state is determined by computing the fourth-order Jacobian matrix as follows:

$$J_4 = \begin{pmatrix} 1 - V_e^2 - k_0(\alpha + \beta\phi^2) & -1 & 1 & -2k_0\beta V_e\phi_e \\ P_4 & -P_2P_4 & 0 & 0 \\ -P_5 & 0 & -P_5 & 0 \\ k_1 & 0 & 0 & -k_2 \end{pmatrix}. \quad (11)$$

The characteristic equation is now quartic $\det(J_4 - \Lambda I_4) = 0$:

$$\Lambda^4 + B_3\Lambda^3 + B_2\Lambda^2 + B_1\Lambda + B_0 = 0. \quad (12)$$

If we define:

$$C = 1 - V_e^2 - k_0(\alpha + \beta\phi^2), \quad D = 2k_0\beta V_e\phi_e. \quad (13)$$

then:

$$B_3 = k_2 + P_5 + P_2P_4 - C,$$

$$B_2 = P_4 + P_5 + k_2P_5 + k_1D - (C - P_2P_4)(k_2 + P_5) - CP_2P_4,$$

$$B_1 = P_4(k_2 + P_5) + P_5(P_2P_4 + k_2) + Dk_1(P_2P_4 + P_5) - CP_2P_4(k_2 + P_5) - k_2P_5(C - P_2P_4),$$

$$B_0 = P_2P_4P_5(1 + k_2) + P_2P_4P_5(k_1D - k_2C). \quad (14)$$

To find the Hopf bifurcations, we substitute $\Lambda = 1\Omega$ into Eq. (12) and equate real and imaginary parts. This gives Ω^2 a common positive root of $\Omega^4 - B_2\Omega^2 + B_0 = 0$ and $\Omega^2 = \frac{B_1}{B_3}$. When both conditions hold, we can omit Ω to obtain the following:

$$B_1^2 - B_1B_2B_3 + B_0B_3^2 = 0. \quad (15)$$

Again, the complexity of the coefficients, with two control parameters found in the fixed point expression,

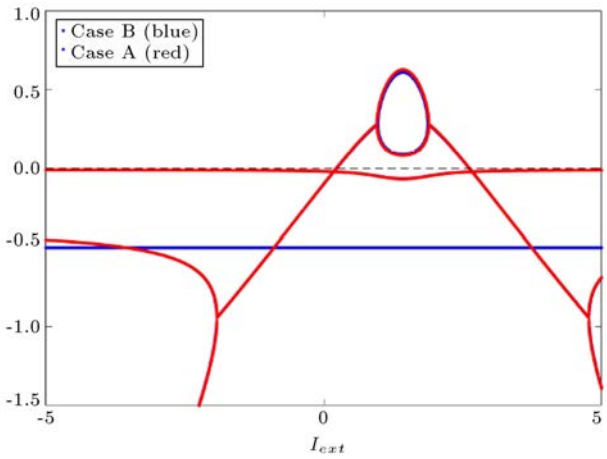

Figure 8. Comparison of the real eigenvalues for Case B (blue) and Case A (red) as I_{ext} increases.

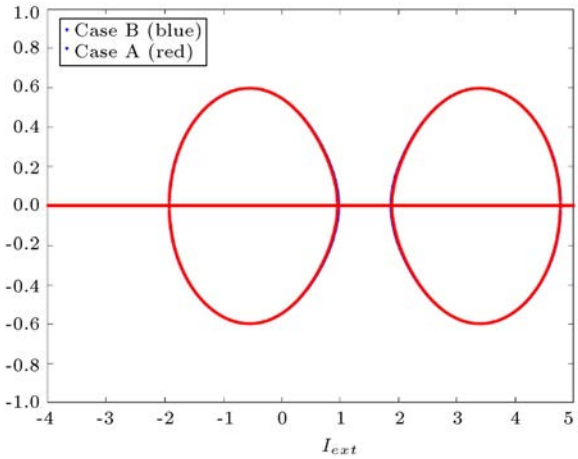

Figure 9. Comparison of the imaginary parts of the eigenvalues for Cases A (red) and B (blue) as I_{ext} increases.

renders an analytical solution extremely cumbersome. Therefore, we rely on numerical integrations to determine the eigenvalues.

Figure 8 shows a comparison between the real eigenvalues for Case B (blue) and the corresponding real eigenvalues for Case A as I_{ext} increases.

Except for additional curves susceptible to ϕ variation, the curves are almost identical. The locations of the Hopf bifurcations are shifted slightly to HB_1 at $I_{ext} = 0.23$ and HB_2 at $I_{ext} = 2.62$. The frequencies of bifurcating periodic limit cycles are both equal to $\Omega = 0.49238$. Figure 9 shows the corresponding plots for the imaginary eigenvalues in both cases.

Figure 10 shows analogous plots when c increases. The two Hopf bifurcation points are located at $c = -1.054$ for HB_1 and at $c = 1.344$ for HB_2 with frequencies $\Omega = 0.492476$ for the chosen set of parameter values, and the linear eigenvalues are -0.5, -0.0362, and $0.2013 \pm 0.2784i$.

4. Bifurcation diagram analysis

Complete dynamical behavior of the system can be investigated by exploring the impact of FH-R model parameters. The bifurcation diagrams are derived for two cases (A and B) and are analyzed.

4.1. Bifurcation of the FH-R model for Case A (without magnetic induction)

First, the bifurcation of the FH-R system without magnetic induction is done. By considering c as the control parameter, other parameters are the same as those in Eq. (2). The dynamical behavior in the bifurcation diagram with respect to the parameter c is shown in Figure 11(a). The parameter c varies from $[-0.6, 0]$ and the local maxima of v are plotted. Different behaviors such as limit cycle, period doubling, and chaotic oscillation in this parameter range can be observed. The density of chaotic regions also varies while the parameter c increases. Both the period-doubling route to chaos and period halving exit from chaos can be detected.

Two different colors in Figure 11(a) correspond to the forward (blue plot) and backward (red plot) continuations. To plot blue dots, the parameter c increases from -0.6 to 0. While for plotting the bifurcation diagram corresponding to red dots, the parameter c decreases from 0 to -0.6. In both cases, initial conditions are chosen from the end values of the states at each step. The maximum peaks of the variable v are chosen to be plotted in both red and blue dots in each step. Differences between the two bifurcation diagrams point to multi-stability of the neuron model, which is confirmed by plotting the corresponding Lyapunov exponent diagrams in Figure 11(b). The Wolf algorithm is used for calculating the Lyapunov exponent in diagrams [39].

4.2. Bifurcation of FH-R model for Case B (with magnetic induction)

The second step is dedicated to Case B. In this case, the neuron model is exposed to magnetic induction. The control parameter for bifurcation is excitation current I_{ext}, while the other parameters are the same as those in Eq. (8). The bifurcation diagram is presented in Figure 12(a). The parameter I_{ext} ranges between $[0.25, 0.75]$ for the analysis and the local maximum of is plotted. The limit cycle, period doubling, and chaotic oscillation with this parameter range can be observed. Interestingly, the density of the chaotic region varies while the parameter increases. The property of Antimonotonicity can be clearly seen in the diagram, which has not been observed in earlier studies.

The same as those in Figure 11(a), two different colors are chosen to correspond to the forward (blue plot) and backward (red plot) continuation. To plot

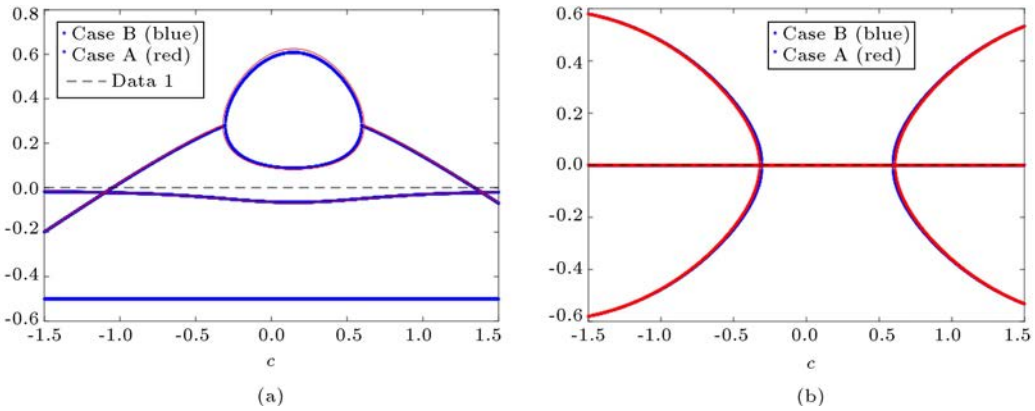

Figure 10. (a) Both the real eigenvalues for Case B (blue) and Case A (red) as c increases. (b) Both the imaginary parts of the eigenvalues for Cases A and B as c increases.

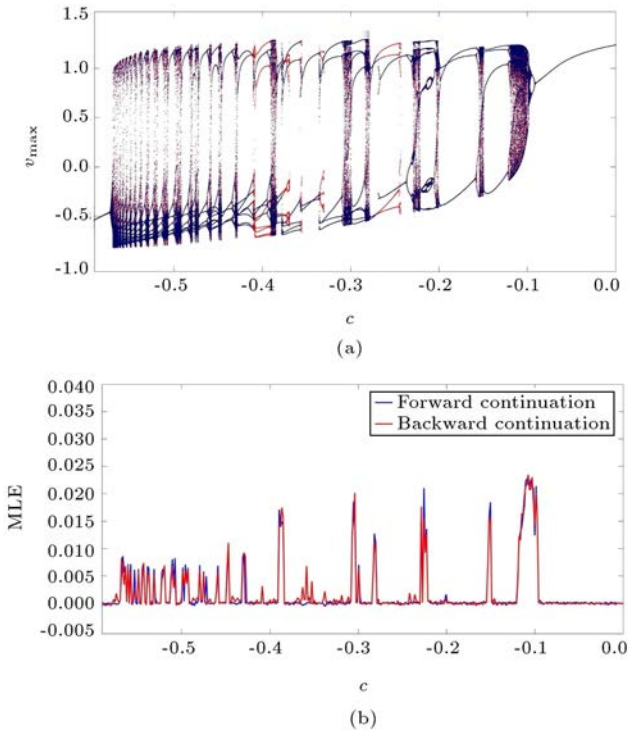

Figure 11. (a) Bifurcation of the FitzHugh-Rinzel (FH-R) neuron model with c using forward and backward continuation shown in blue and red plots, respectively. (b) The corresponding maximum Lyapunov exponents for forward and backward continuation.

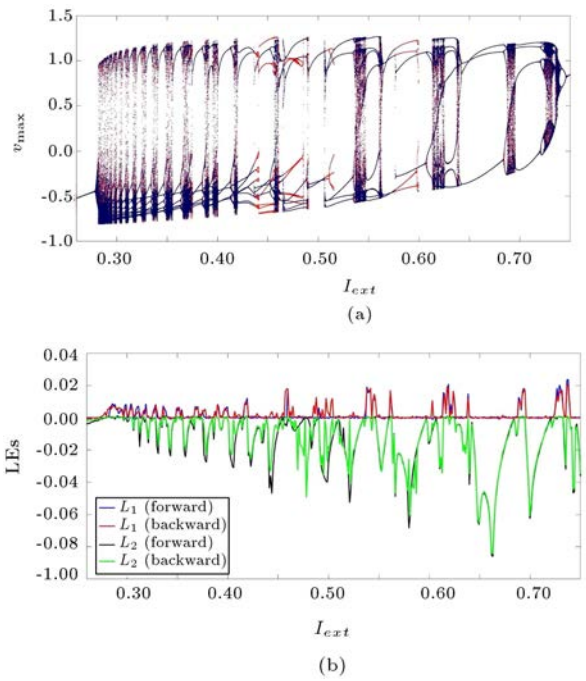

Figure 12. (a) Bifurcation of the FitzHugh-Rinzel (FH-R) neuron model with I_{ext} using forward and backward continuation shown in blue and red plots, respectively. (b) The corresponding maximum Lyapunov exponents for forward and backward continuation.

blue dots, the parameter c increases from 0.25 to 0.75. However, for plotting the bifurcation diagram corresponding to red dots, the parameter c decreases from 0.75 to 0.25. In both cases, the initial conditions are chosen from the end values of the states at each step. The maximum peaks of the variable v are selected to be plotted in each step in both red and blue dots. Differences between the two bifurcation diagrams point to the existence of the multi-stability of the neuron model, which is confirmed by plotting the corresponding Lyapunov exponent in Figure 12(b).

5. Spatiotemporal dynamics of the FH-R neuron network

After investigating the local kinetics of the FH-R model, it is now time we discussed the complex network behavior of the FH-R model. In this respect, a network is constructed by 110 × 110 FH-R neurons whose local kinetics is governed by Eq. (1) for both Case A and Case B with Neumann boundary conditions. To explore the propagation of waves in the network, an external stimulus ($A\sin(\omega t)$) is exposed to the center of the network. The initial states of the variables are set to (0,0,0) for Case A and (0,0,0,0.5) for Case B. The

FH-R neuron network of 110×110 size can be defined as follows:

$$Case\ A: \begin{cases} \dot{v}_{ij} = v_{ij} - \frac{v_{ij}^3}{3} - w_{ij} + y_{ij} + I_{ext} \\ \quad +D(v_{i+1j} + v_{i-1j} + v_{ij+1} \\ \quad +v_{ij-1} - 4v_{ij}) + \chi(t)\psi_{i\theta_1}\psi_{j\theta_2} \\ \dot{w}_{ij} = \delta(0.7 + v_{ij} - 0.8w_{ij}) \\ y_{ij} = \mu(c - y_{ij} - v_{ij}) \end{cases} \quad (16)$$

$$Case\ B: \begin{cases} \dot{v}_{ij} = v_{ij} - \frac{v_{ij}^3}{3} - w_{ij} + y_{ij} + I_{ext} \\ \quad -k_0 v(\alpha + \beta\phi^2) + D(v_{i+1j} \\ \quad +v_{i-1j} + v_{ij+1} + v_{ij-1} - 4v_{ij}) \\ \quad +\chi(t)\psi_{i\theta_1}\psi_{j\theta_2} \\ \dot{w}_{ij} = \delta(0.7 + v_{ij} - 0.8w_{ij}) \\ y_{ij} = \mu(c - y_{ij} - v_{ij}) \\ \phi_{ij} = k_1 v_{ij} - k_2\phi_{ij} \end{cases} \quad (17)$$

where D shows the electrical coupling strength. $\chi(t) = A\sin(\omega t)$ is the external stimuli that are applied to the network when $\xi_{i\theta_1} = 1, \xi_{i\theta_2} = 1$ for $i = \theta_1 = 55, j = \theta_2 = 55$, respectively. The parameter values in Eq. (16) are $I_{ext} = 0.73, \delta = 0.01, \mu = 0.35, c = -0.55$ and $\alpha = 0.1, \beta = 0.03, k_0 = 0.1, k_1 = 0.01, k_2 = 0.5$ are the additional parameters required for (20).

The spatiotemporal behavior of the first variable of the model is explored, and the final patterns at $t = 3000$ are shown. The entire discussion is first subdivided into Case A and Case B and in each case, we have discussed the impact of the diffusion coefficient and stimuli parameter (frequency/amplitude).

5.1. Case A (without magnetic induction)

The spatiotemporal pattern of the neuron model without considering the effect of magnetic induction is investigated in three steps. At first, the effect of coupling strength (D) is explored when the amplitude and frequency of the external stimuli are set to $A = \omega = 1$. Figure 13 exhibits wave propagation in the network in the case of five different coupling strength degrees.

According to the results in Figure 13, it can be concluded that increasing the coupling strength leads to the emergence of highly ordered patterns. For instance, the small value of the coupling strength in Figure 13(a) ends with irregular patterns. Upon further increase in the coupling strength (Figure 13(b) (c), and (d)), some seeds in the waves appeared in the network, which were getting stronger. Finally, when the coupling strength was set to $D = 1$, strong regular waves formed in the network.

In the second step, the frequency effect of the stimuli on the emergence of the network's spatiotemporal pattern is investigated. Accordingly, the frequency of the external stimuli increases smoothly and the spatiotemporal pattern of the network is plotted in Figure 14.

Figure 14 shows the effect of the frequency of external stimuli on wave propagation in the network.

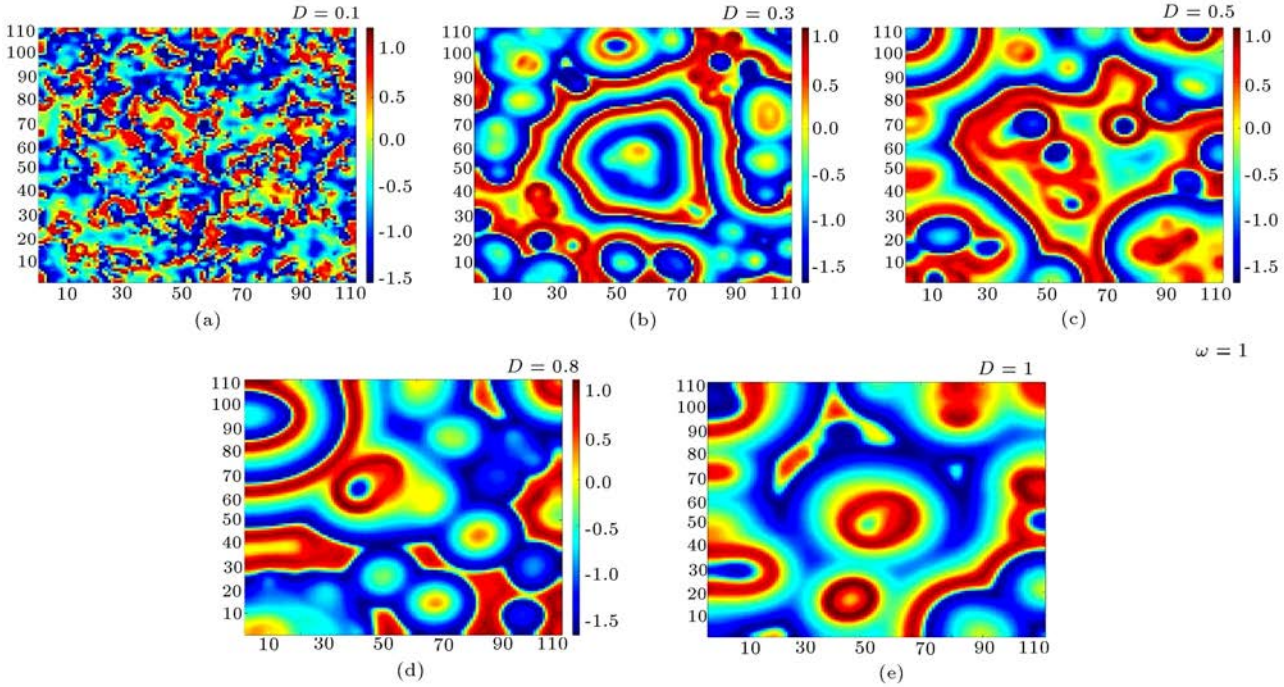

Figure 13. The spatiotemporal behavior of the network for five different coupling strengths: (a) $D = 0.1$, (b) $D = 0.3$, (c) $D = 0.5$, (d) $D = 0.8$, and (e) $D = 1$. Wave propagation in the network with small coupling strength is more irregular than the network with larger coupling strength.

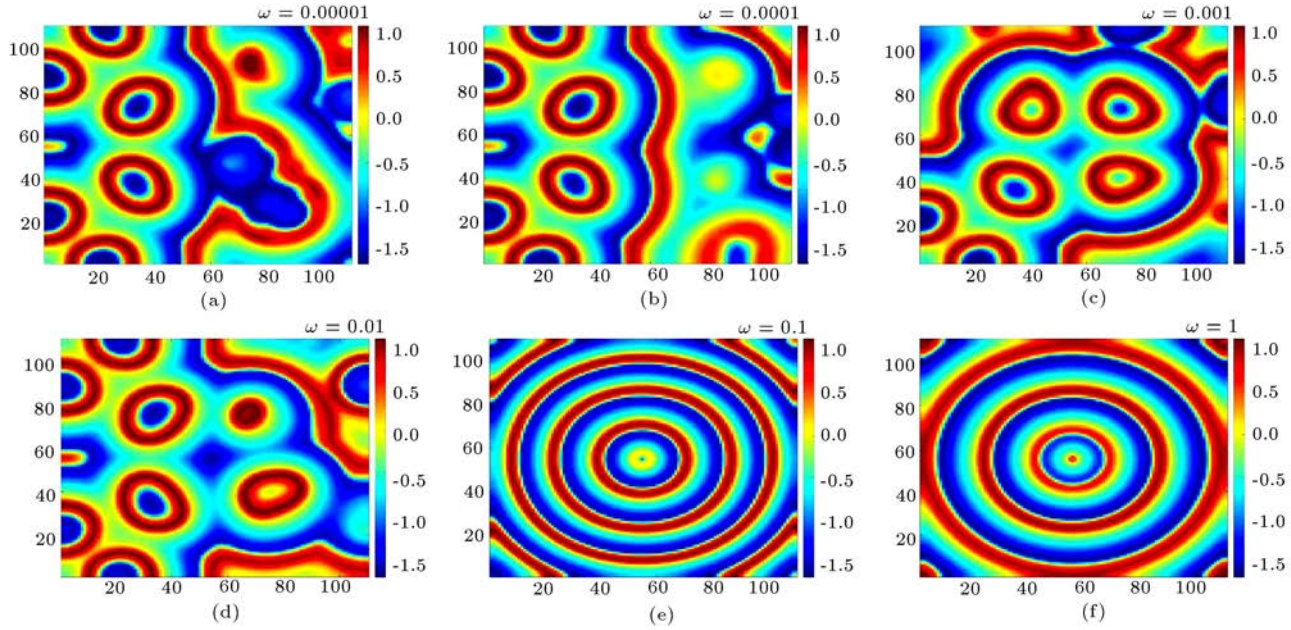

Figure 14. The spatiotemporal behavior of the network (Case A) for six different frequencies: (a) $\omega = 0.00001$, (b) $\omega = 0.0001$, (c) $\omega = 0.001$, (d) $\omega = 0.01$, (e) $\omega = 0.1$, and (f) $\omega = 1$. For smaller frequencies, more wave seeds are propagating irregularly. However, increasing the external stimuli's frequencies leads to lower wave seeds with more regular wave propagation in the network.

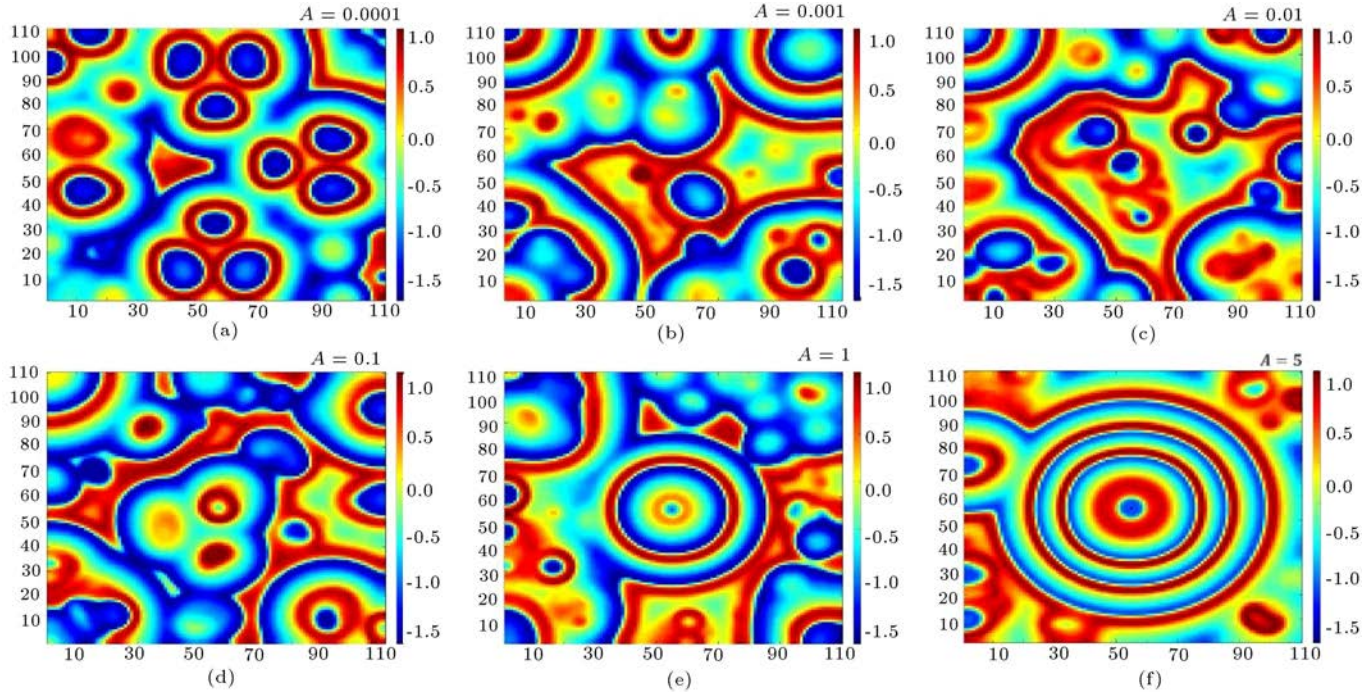

Figure 15. The spatiotemporal behavior of the network for six different amplitudes (a) $A = 0.0001$, (b) $A = 0.001$, (c) $A = 0.01$, (d) $A = 0.1$, (e) $A = 1$, and (f) $A = 5$. The amplitude of the external stimuli does not have a concrete effect on wave propagation on the network.

It can be implied that the wave seeds in the network under stimuli with low frequency propagate irregularly. However, if the frequency exceeds a specific threshold ($\omega = 0.1$), the wave propagation turns periodic on the network.

The last step concerns the amplitude of the external stimuli as a varying parameter to study the spatiotemporal pattern of the network. The overall behavior of the network is examined based on six different amplitude values in Figure 15.

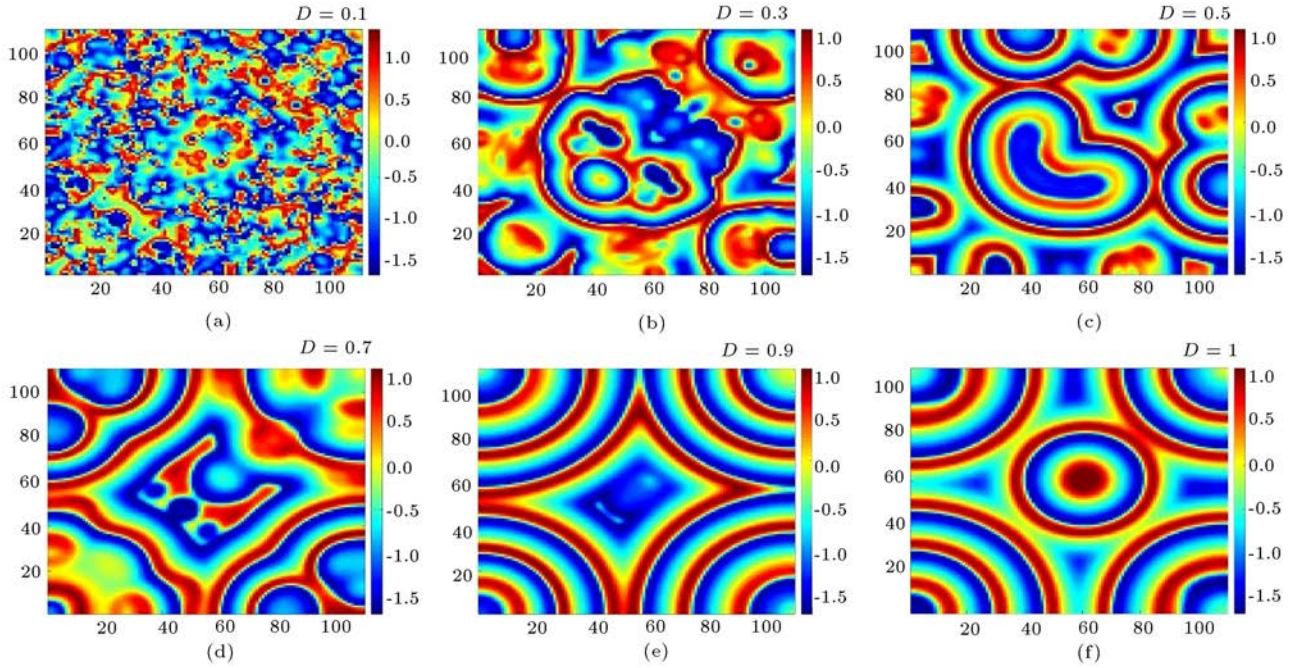

Figure 16. The spatiotemporal behavior of the network (Case B) for six different coupling strengths: (a) $D = 0.1$, (b) $D = 0.3$, (c) $D = 0.5$, (d) $D = 0.7$, (e) $D = 0.9$, and (f) $D = 1$. The larger the coupling strength is, the more regular the waves propagate in the network.

Changing the amplitude of external stimuli can affect the behavior of the network. Figure 15 shows the final patterns of the network at $t = 3000$ according to six different amplitude values. The irregular pattern of wave propagation can be seen in the network at an amplitude value below $A = 1$. However, the network would switch to regular and periodic modes at a larger amplitude value. A comparison of results of the network spatiotemporal pattern based on the three factors revealed that wave propagation in the network was almost affected by coupling strength and the frequency of external stimuli rather than the amplitude.

5.2. Case B (with magnetic induction)

Similar to the last section, the coupling strength and parameters of the external stimuli are considered as the main effective factors in the spatiotemporal behavior of the network. According to the results shown in Figure 15, the amplitude of the network cannot be considered an effective parameter for wave propagation. In this respect, the impact of coupling strength and frequency of the external stimuli on the emergence and propagation of seed waves was investigated. Accordingly, this section can be divided into two steps: the first devoted to the impact of coupling strength and the second to investigating the effect of the frequency of the stimuli. Figure 16 shows the spatiotemporal patterns of six different coupling strengths.

Similar to Case A, increase in the coupling strength of the network in Case B leads to highly ordered patterns. Comparing the results of Figure 16 with Figure 13 reveals that the effect of the coupling strength on wave propagation in the network of Case B is greater than that in Case A.

In the second step, the spatiotemporal network patterns for six different frequencies of the external stimuli are shown in Figure 17.

For $\omega = 0.0001$ in Figure 17(a), periodic waves propagate in the network and the spatiotemporal pattern of the network is regular. Increasing the frequency in the range of $0.0001 < \omega < 0.1$ disturbs the network regularity and leads to irregular wave propagation. However, the network returns to the periodic wave propagation mode in the case of $\omega = 0.1$. Further increases in the frequency of the stimuli would retrieve the irregular wave propagation in the network again. Therefore, the overall conclusion is that in contrast with the result of Case A, increasing the frequency of the external stimuli has an inverse effect on propagation of regular waves on the network.

6. Conclusion

This paper compared the dynamical behavior of the modified FitzHugh-Rinzel (FH-R) neuron model exposed to the magnetic field (Case B) with that of the FH-R model (Case A). To this end, the stability of the equilibrium points was studied in both models. Appropriate criteria for detecting Hopf bifurcation were evaluated. Exploring the bifurcation diagram and Lyapunov exponent diagrams revealed that both Case A and Case B categorized the systems with

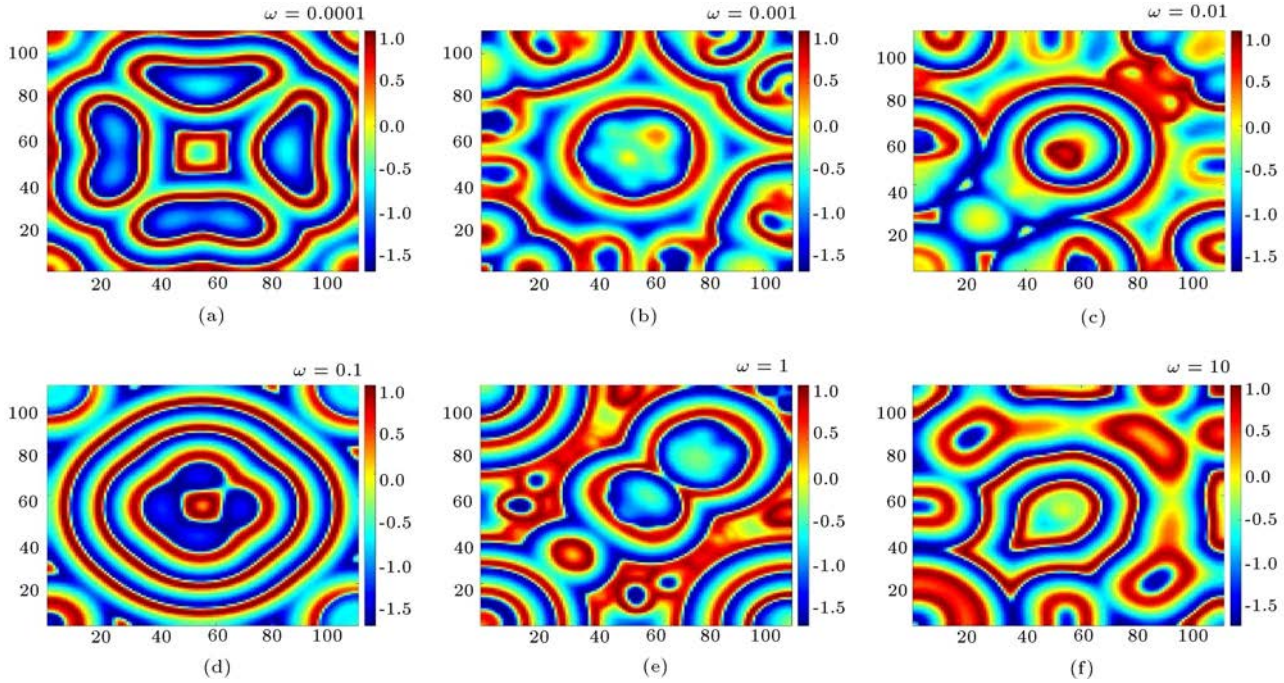

Figure 17. The spatiotemporal behavior of the network (Case B) for six different frequencies: (a) $\omega = 0.0001$, (b) $\omega = 0.001$, (c) $\omega = 0.01$, (d) $\omega = 0.1$, (e) $\omega = 1$, and (f) $\omega = 10$. The frequency of the external stimuli in Case B has an inverse effect on producing regular waves on the network. The larger frequencies lead to irregular wave propagation in the network.

multi-stability. Also, the dynamical behavior of the network consisting of the 110×110 FH-R neuron model was investigated. The effects of coupling strength, frequency, and amplitude of external stimuli on the emergence and propagation of the waves in the network were reported in neuron models of Cases A and B. The results demonstrated that increasing coupling strength led to a more regular wave pattern. However, the effect of coupling strength on the emergence of the regular wave patterns in Case B was more efficient than that in Case A. The frequency of the external stimuli effect on the spatiotemporal behavior of the network was different in Case A and Case B. In Case A, increasing the frequency of external stimuli led to more regular wave propagation in the network. In contrast, the effect of the frequency of external stimuli in Case B produced more irregular waves in the network at larger frequencies. Moreover, the amplitude of external stimuli did not have any significant effect on the network's wave propagation in both cases.

References

1. Skarda, C.A. and Freeman, W.J. "Chaos and the new science of the brain", *Concepts in Neuroscience*, **1**(2), pp. 275–285 (1990).
2. Kim, J.H. and Stringer, J., *Applied Chaos*, New York, NY: John Wiley and Sons, Inc. (1992).
3. Hodgkin, A.L. and Huxley, A.F. "Quantitative description of membrane current and its application to conduction and excitation in nerve", *J. Physiol*, **117**(4), pp. 500–544 (1952).
4. Ma, J. and Tang, J. "A review for dynamics of collective behaviors of network of neurons", *Sci. China Technol*, **58**, pp. 2038–2045 (2015).
5. Hindmarsh, J.L. and Rose, R.M. "A model of neuronal bursting using three coupled first order differential equations", *Proc. Roy. Soc. London B*, **221**, pp. 87–102 (1984).
6. Bao, B., Zhu, Y., Ma, J., et al. "Memristive neuron model with an adapting synapse and its hardware experiments", *Science China Technological Sciences*, pp. 1–11 (2021).
7. Xu, Y., Ma, J., Zhan, X., et al. "Temperature effect on memristive ion channels", *Cognitive Neurodynamics*, **13**(6), pp. 601–611 (2019).
8. Xu, Y., Guo, Y., Ren, G., et al. "Dynamics and stochastic resonance in a thermosensitive neuron", *Applied Mathematics and Computation*, **385**, p. 125427 (2020).
9. Liu, Y., Xu, W.J., Ma, J., et al. "A new photosensitive neuron model and its dynamics", *Frontiers of Information Technology & Electronic Engineering*, **21**, pp. 1387–1396 (2020).
10. Xu, Y., Liu, M., Zhu, Z., et al. "Dynamics and coherence resonance in a thermosensitive neuron driven by photocurrent", *Chinese Physics B*, **29**(9), p. 098704 (2020).
11. Zhou, P., Yao, Z., Ma, J., et al. "A piezoelectric sensing neuron and resonance synchronization between

auditory neurons under stimulus", *Chaos*, Solitons & Fractals, **145**, p. 110751 (2021).

12. Wang, Y., Ma, J., Xu, Y., et al. "The electrical activity of neurons subject to electromagnetic induction and Gaussian white noise", *International Journal of Bifurcation and Chaos*, **27**(2), pp. 1750030–1750042 (2017).
13. FitzHugh, R. "Impulses and physiological states in theoretical models of nerve membrane", *Biophys. J.*, **1**(6), pp. 445–466 (1961).
14. Nagumo, J., Arimoto, S., and Yoshizawa, S. "An active pulse transmission line simulating nerve axon", *Proc. of the IRE*, **50**(10), pp. 2061–2070 (1962).
15. Pouryahya, S. "Nonlinear dynamics, synchronisation and chaos in coupled FHN cardiac and neural cells", Ph.D., National University of Ireland Maynooth (2013).
16. Guckenheimer, J. and Kuehn, C. "Homoclinic orbits of the FitzHugh-Nagumo equation: Bifurcations in the full system", *SIAM J. Appl. Dynam. Syst.*, **9**(1), pp. 138–153 (2010).
17. Hoff, A., dos Santos, J.V., Manchein, C., et al. "Numerical bifurcation analysis of two coupled FitzHugh-Nagumo oscillators", *Eur. Phys. J. B*, **87**(7), pp. 1–9 (2014).
18. Pal, K., Ghosh, D., and Gangopadhyay, G. "Synchronization and metabolic energy consumption in stochastic Hodgkin-Huxley neurons: Patch size and drug blockers", *Neurocomputing*, **422**, pp. 222–234 (2021).
19. Doss-Bachelet, C., Françoise, J.P., and Piquet, C. "Bursting oscillations in two coupled FitzHugh-Nagumo systems", *ComPlexUs*, **1**(3), pp. 101–111 (2003).
20. Majhi, S. and Ghosh, D. "Alternating chimeras in networks of ephaptically coupled bursting neurons", *Chaos: An Interdisciplinary Journal of Nonlinear Science*, **28**(8), p. 083113 (2018).
21. Bera, B.K., Rakshit, S., Ghosh, D., et al. "Spike chimera states and firing regularities in neuronal hypernetworks", *Chaos: An Interdisciplinary Journal of Nonlinear Science*, **29**(5), p. 053115 (2019).
22. Makarov, V.V., Kundu, S., Kirsanov, D.V., et al. "Multiscale interaction promotes chimera states in complex networks", *Communications in Nonlinear Science and Numerical Simulation*, **71**, pp. 118–129 (2019).
23. Ciszak, M., Euzzor, S., Arecchi, F.T., et al. "Experimental study of firing death in a network of chaotic FitzHugh-Nagumo neurons", *Phys. Rev. E*, **87**(2), 022919(022911-022917) (2013).
24. Gray, C.M. and McCormick, D.A. "Chattering cells: superficial pyramidal neurons contributing to the generation of synchronous oscillations in the visual vortex", *Science*, **274**(5284), pp. 109–113 (1996).
25. Kudryashov, N.A. "Asymptotic and exact solutions of the FitzHugh-Nagumo model", *Regular and Chaotic Dynamics*, **23**(2), pp. 152–160 (2018).
26. Tehrani, N.F. and Razvan, M. "Bifurcation structure of two coupled FHN neurons with delay", *Mathematical Biosciences*, **270**, pp. 41–56 (2015).
27. Zemlyanukhin, A.I. and Bochkarev, A.V. "Analytical properties and solutions of the FitzHugh-Rinzel model", *Russian Journal of Nonlinear Dynamics*, **15**(1), pp. 3–12 (2019).
28. Wojcik, J. and Shilnikov, A., *Voltage Interval Mappings for an Elliptic Bursting Model*, **12**, Springer, Cham (2015).
29. Belykh, V.N. and Pankratova, E.V. "Chaotic synchronization in ensembles of coupled neurons modeled by the FitzHugh-Rinzel system", *Radiophys. Quantum El.*, **49**(11), pp. 910–921 (2006).
30. Shima, S.I. and Kuramoto, Y. "Rotating spiral waves with phase-randomized core in nonlocally coupled oscillators", *Phys. Rev. E*, **69**, p. 036213 (2004).
31. Kuramoto, Y. and Shima, S.I. "Rotating spirals without phase singularity in reaction-diffusion systems", *Progr. Theor. Phys. Suppl*, **150**, p. 115 (2003).
32. Kuramoto, Y., Shima, S.I., Battogtokh, D., et al. "Mean-field theory revives in self-oscillatory field with Non-Local coupling", *Prog. Theor. Phys. Suppl*, **161**, p. 127 (2006).
33. Brooks, H.A. and Bressloff, P.C. "Quasicycles in the stochastic hybrid Morris-Lecar neural model", *Physical Review E*, **92**, p. 012704 (2015).
34. Hou, Z. and Xin, H. "Noise-sustained spiral waves: effect of spatial and temporal memory", *Phys Rev Lett*, **89**, p. 280601 (2002).
35. Mondal, A., Sharma, S.K., Upadhyay, R.K., et al. "Firing activities of a fractional-order FitzHugh-Rinzel bursting neuron model and its coupled dynamics", *Sci Rep*, **9**, p. 15721 (2019).
36. Rinzel, J. "A formal classification of bursting mechanisms in excitable systems, in mathematical topics in population biology", *Morphogenesis and Neurosciences, Lecture Notes in Biomathematics*, **71**, pp. 267–281 (1987).
37. Rinzel, J. and Troy, W.C. "Bursting phenomena in a simplified oregonator flow system model", *J Chem Phys*, **76**, pp. 1775–1789 (1982).
38. Lv, M., Wang, C., Ren, G., et al. "Model of electrical activity in a neuron under magnetic flow effect", *Nonlinear Dyn.*, **85**, pp. 1479–1490 (2016).
39. Wolf, A., Swift, J.B., Swinney, H.L., et al. "Determining Lyapunov exponents from a time series", *Physica D: Nonlinear Phenomena*, **16**(3), pp. 285–317 (1985).

Biographies

Zhen Wang was born in Shaanxi, China, in 1981. He received the BS degree and MS degree in 2004 and 2008 respectively from Shaanxi University of Science and Technology, China. He is currently a Professor of School of Science at Xijing University. His research

interests include ordinary differential equations and dynamical systems, nonlinear control system theory etc.

Peijun Zhang was born in Taihu of Anhui Province, China, in 1984, and graduated from school of mathematics and statistics of Lanzhou University with a master's degree of science. He is mainly engaged in the study of ordinary differential equations and dynamical systems. He is now working in the school of science of Xijing University.

Irene Moroz graduated with a Class I in Mathematics from Oxford University in 1977. She then received her PhD on slowly varying baroclinic waves from Leeds University, UK in 1981. After spending 2 years as a post-doctoral fellow in Leeds, she spent 18 months as a Visiting Assistant Professor at Cornell University, before taking up a New Blood Lectureship at the University of East Anglia in 1985. Since 1992, she has been a Fellow in Applied Maths at St Hilda's College. Her research interests include nonlinear dynamical systems applied to mathematical ecology, geophysical fluid dyanmics, dynamo models and climate modelling.

Anitha Karthikeyan is presently working as Professor in Department of Electronics and Communication Engineering, Prathyusha Engineering College, Chennai, India. She has completed her PhD in Electronics and Communication Engineering with specializing in Discrete Maps based Random number generators. Her post-graduation was in embedded system technologies with emphasis on real-time targets programming. She has over 80 international journal papers indexed in SCI and her present research areas include fractional order nonlinear systems and control, time delay systems, FPGA and LabVIEW implementations of fractional order systems.